Molecular Dynamics Simulation of Polymer Liquid and Glass. 4. Free-Volume Distribution

D. Rigby† and R. J. Roe*

Department of Materials Science and Engineering, University of Cincinnati, Cincinnati, Ohio 45221

Received March 29, 1990; Revised Manuscript Received June 8, 1990

ABSTRACT: Molecular dynamics simulation has been performed with dense systems of alkane-like chain molecules subject to potentials restricting bond lengths, bond angles, and trans–gauche torsional angles and interacting with neighboring chains according to a truncated Lennard-Jones potential. Distribution of occupied and unoccupied space in the system was then evaluated by the technique of Voronoi tessellation of space and by enumeration of the cavities formed when hard spheres of diameter D were assumed placed on atomic centers. The distribution of volumes of Voronoi polyhedra is broad at high temperatures but becomes narrower as the temperature is lowered through the T_g. The polyhedra associated with chain and segments are generally much larger than those associated with internal segments. The distribution of cavity volumes is extremely broad and often exhibits a bimodal or trimodal character. The overall volume fraction of cavities in the system decreases when the temperature is lowered toward the T_g, below which the rate of decrease is greatly reduced; the overall behavior thus parallels the change in the total volume with temperature. The number density of cavities either increases or decreases on cooling, depending on the value of the diameter D, but remains fairly constant at temperatures below the T_g. These cavities change shape and size with time; even at temperatures much below the T_g, persistent low-frequency, large-amplitude molecular motions produce waxing and waning of the cavities. The reappearance of a cavity at the position from which it disappeared earlier suggests the existence of spatial inhomogeneity in density, which does not decay on the time scale of our simulation.

Introduction

Understanding the nature of the glassy state and glass transition is one of the long-standing problems of materials science and physics. A variety of experimental techniques are utilized toward this end. The modeling of glass structures by means of computer simulation is a powerful new technique emerging with much promise. The method will enable many new types of "measurements" to be performed to evaluate properties of glasses that conventional laboratory experiments cannot easily provide. The distribution of free volume, investigated in this work, is such an example.

The concept of free volume has long been utilized to explain glass transition phenomena and the behavior of glassy materials. The concept is widely accepted by many because of its simplicity and intuitive plausibility. The extent of availability of unoccupied space surrounding a particle (molecule) is easily visualized as playing a key role in determining the mobility of the particle. The viscosities of hydrocarbon liquids were successfully correlated on this basis.[1] The chain-length dependence of the glass transition temperature of polymers was explained by an assumed larger free volume surrounding a chain end.[2] The glass transition points of different materials were then thought of as representing an iso-free-volume state.[3] The physical aging,[4] i.e., stiffening and embrittlement of glassy materials left standing below the T_g, can naturally be associated with the accompanying slow decrease[5] in specific volume and hence in free volume.

Despite its usefulness, some inadequacies of the concept of free volume have also been recognized in many instances. The fact that properties of glassy materials depend on previous mechanical and thermal histories and not merely on the current state (the current value of specific volume, for example) is well-known. This means either that the free volume is not uniquely determined even when the current total volume is given, or alternatively that the observed properties depend on some other quantities in addition to free volume. This has led to the suggestion that not only the total free volume content but also the distribution of free volume may have to be known to explain observed phenomena. Consequently, there have recently been some efforts to determine the free-volume distribution by experimental techniques, utilizing for example the annihilation of positrons[6] and the kinetics[7,8] of isomerization of probe molecules added to glassy polymers. These experimental techniques are laborious and also involve some ambiguities in interpreting the results quantitatively in terms of free-volume distribution. Computer modeling of glassy materials provides an alternative method of evaluating free-volume distribution under a variety of conditions, rather readily and perhaps with less ambiguity.

The versatility of the concept of free volume arises in part, paradoxically, from its ambiguity. No unique, quantitative definition of free volume, accepted by all the workers in the field, is really available. The free volume is often defined in a subtly different way to accommodate the need to interpret a particular phenomenon under consideration. Similarly, for the evaluation of the free volume and its distribution from molecular models obtained by computer simulation, a number of different approaches are conceivable, of which the following three are the most obvious. In the first, the atoms are replaced by hard spheres of van der Waals radius or some similarly defined radius. Any space that is not covered by any of these overlapping hard spheres is then considered free volume. Here a correct choice of the hard-sphere radius is important. Whether the radius is to depend on temperature (to allow for vibrational amplitudes varying with temperature) is a difficult choice to make. In the second approach, the technique of Voronoi[9] tessellation of space is utilized. The space is subdivided into space-filling convex polyhedra surrounding each atom. Given the positions of atomic centers, Voronoi polyhedra are

† Present address: Biosym Technologies, Inc., 10065A Barnes, Canyon Road, San Diego, CA 92121.

0024-9297/90/2223-5312$02.50/0

unambiguously defined, and the distribution of free volume can be discussed by reference to the size distribution of these polyhedra, thus side-skirting the issue of the correct atomic radius to use. In the third approach, the free volume, v_f, surrounding an atom i is defined[10,11] by

$$v_f = \int \exp[-\phi_i(r)/kT + \phi_i(r_0)/kT]\, dr \qquad (1)$$

where $\phi_i(r)$ is the potential energy that would act on atom i, if it were placed at position r while keeping all the surrounding atoms at their respective positions, and r_0 is the position of the local potential energy minimum. The above definition, originally developed for analysis of monatomic liquids, needs a modification for the study of polymer liquids in view of the presence of covalently bonded neighbors along the chain.

In this work the first two of the above three schemes of analyzing free-volume distribution are applied to the study of the structure of alkane-like liquid and glass that we have obtained by a molecular dynamics simulation. In addition to evaluating various static measures of free-volume distribution, we have also made some preliminary study of the dynamics of free-volume fluctuation taking place in the glassy state, showing that a considerable degree of change in the shape and size of free-volume cavities is observable even within the time scale of our simulation.

The main results of our molecular dynamics simulation on systems of n-alkane-like molecules have been presented in previous publications.[12-15] Some salient features of our findings are as follows. On stepwise cooling under constant pressure, the system undergoes a transition possessing many of the characteristics of the laboratory glass transition. Thus we find discontinuities in the temperature coefficients of the density and internal energy at a temperature that increases with increasing chain length. At slightly higher temperatures, bond conformational transitions cease, leading to a freezing of chain dimensions and shapes, while at slightly lower temperatures translational diffusion of chain segments is arrested.[12] A further detailed analysis of chain packing and orientation correlation in these systems by means of radial distribution functions and spatial orientation correlation functions for short sequences of the molecules revealed that an appreciable degree of short-range order exists in the packing of chains.[13] The degree of orientation correlation between chains showed a rapid improvement as the system was cooled toward the glass transition temperature, and this continued to occur, though at a reduced rate, below the T_g. When annealing was performed just above the T_g, the orientation correlation showed a large increase with time as the system underwent a transition to an orientationally ordered smecticlike state.

Method

The present work uses a united-atom model in which individual n-alkane chains are modeled as sequences of spherical CH_2 (or CH_3) segments. Bond lengths and valence angles vary subject to quadratic potential functions, while preference for the trans rotational state and the rate of conformational transitions between trans and gauche states are controlled by a 3-fold torsional potential. All other interactions, between CH_2 groups separated by more than three bonds along a given chain and between all CH_2 or CH_3 groups in different chains are governed by a truncated and shifted Lennard-Jones 6-12 potential. The forms of the above functions are presented in Table I.

As commonly practiced, we use a system of reduced units, in which the units of length and energy are given by the Lennard-Jones r^* and ϵ^* parameters, and the unit of mass corresponds to the mass of a CH_2 group. These basic units and others derived therefrom are summarized in Table II. All potential function parameters, listed in Table III in both conventional and reduced units, were chosen such that the chains mimic polyethylene, with the exception that the bond stretching force constant was weakened by a factor of ca. 7 to reduce the associated vibrational frequency and thereby allow use of a longer time step when solving the equations of motion for the CH_2 segments.

Table I
Potential Energy Functions Used

bond length
$E_b = (1/2)k_b(l - l_0)^2$
bond angle
$E_\theta = (1/2)k_\theta(\cos\theta - \cos\theta_0)^2$
bond torsion
$E_\phi = k_\phi \sum_{n=0}^{5} a_n \cos^n \phi$
nonbonded interaction
$E_{nb} = 4\epsilon^*[(r^*/r)^{12} - (r^*/r)^6] + C$ for $r < 1.5r^*$
$E_{nb} = 0$ for $r > 1.5r^*$

Table II
Scaling Parameters Used for Expressing Quantities in Reduced Units

energy, ϵ^*	500 J/mol
length, r^*	0.38 nm
mass, m	14 g/mol
temperature, $T^* = \epsilon^*/k$	60.1 K
pressure, $p^* = \epsilon^*/r^{*3}$	15.16 MPa (0.1516 kbar)
time, $t^* = (mr^{*2}/\epsilon^*)^{1/2}$	2.01 ps
density, $\rho^* = 1/r^{*3}$	18.22 nm^{-3} (0.424 g/cm^3)

Table III
Constants Used for Potential Functions

	in reduced units	in absolute units
l_0	0.4	0.152 nm
$\cos\theta_0$	−0.3333	−0.3333
k_b	10^4	3.46×10^7 J/nm^2 mol
k_θ	10_3	5×10^5 J/mol
k_ϕ	18	9000 J/mol
a_0	1	1
a_1	1.3100	1.3100
a_2	−1.4140	−1.4140
a_3	−0.3297	−0.3297
a_4	2.8280	2.8280
a_5	−3.3943	−3.3943
ΔE_{tg}	5.68	2842 J/mol
t-g barrier	23.96	11 978 J/mol
cis barrier	86.89	43 444 J/mol

The bulk system consists of a cubic box with the customary periodic boundary conditions.[16] The calculations reported herein were all performed by using a system containing 25 chains each having 20 segments. The equations of motion of individual segments were integrated numerically by using the Verlet algorithm with a time step of $0.005t^*$ (1.005×10^{-14} s). The stepwise cooling procedure comprises a series of simulations of duration $60t^*$ (ca. 120 ps), each followed by a stepwise reduction in the temperature by $0.2T^*$ (ca. 12 deg) and adjustment of the density to yield the same pressure as the previous run ($p = 3p^*$). At the end of each $60t^*$ segment of the cooling runs, the system configuration was saved and used to start a second run of duration $60t^*$. The free-volume analyses were then performed by using sets of coordinates output at intervals during these longer runs.

All the results reported here pertain to the simulated system in the liquid and glassy states. Occasionally during long simulation runs an onset of crystallization was detected by an anomalous rise in temperature or by the global order parameter (such as the average direction cosines of all bond vectors) failing no longer to vanish completely. In such cases the MD run was restarted from an entirely different configuration of the chains. Since the last configuration of an MD run at a temperature is always used as the starting configuration of the next run at a different temperature, any incipient crystallization, which might have escaped notice in a run, would eventually have manifested itself in the subsequent runs.

As noted in the Introduction, distribution of occupied and unoccupied volumes within the system at various temperatures was examined in two ways. In the first, configurations of the systems were analyzed by replacing each segment by a sphere of diameter D, where the value of the "exclusion diameter" D was

varied from $1.0r^*$ to $2.0r^*$. Any region not occupied by these enlarged "segments" of diameter D thus constitutes a cavity accessible to a probe molecule of diameter $D - D_{vdW}$, where D_{vdW} represents the van der Waals diameter (which may be regarded as approximately equal to $1.0r^*$). To evaluate the cavities, the system was divided into $64 \times 64 \times 64$ cubic cells, each of which was labeled as occupied whenever more than half of its volume lay within one of the spheres of diameter D. A cavity is then defined as a set of connected unoccupied cells. At each temperature, the number of these cavities and their spatial and size distributions were evaluated and averaged over a sequence of 24 configurations output at intervals of 500 integration steps during the run. In addition, a preliminary analysis of the cavity shapes was performed by evaluating distributions of the reduced dimensionless surface-to-volume ratio, w, defined by

$$w = (S/4\pi)/(3V/4\pi)^{2/3} \quad (2)$$

where S and V refer to the cavity surface area and volume, respectively. This parameter has a minimum value of 1.0 for a sphere.

In the Voronoi polyhedra analysis,[17-20] one perpendicularly bisects the vectors connecting all pairs of segments in the system, generating a large number of intersecting planes. The polyhedron associated with a given segment is then obtained by selecting the smallest of the polyhedra thus formed about the chosen segment. Every point within the polyhedron is therefore closer to the chosen segment than to any other segment in the system. In order to characterize the structure of the system in terms of its constituent Voronoi polyhedra, we have evaluated a number of distributions, namely, those of polyhedron volumes, total polyhedron surface areas, and the parameter w defined by eq 2 above, with S and V now referring to the polyhedron surface area and volume. Additionally, we have also monitored distributions of the number of faces per polyhedron and the number of edges per face as the simulated systems are cooled stepwise through the T_g. As in the cavity volume analysis, all distributions have been averaged over a sequence of configurations, in this case output at intervals of 250 steps during the simulation runs.

Results and Discussion

(a) Voronoi Tessellation Analysis. Distributions of volumes of Voronoi polyhedra surrounding individual segments are shown in Figure 1 at temperatures of 5.0, 2.6, 2.0, and 1.0 reduced units. Also illustrated at $T = 5.0$ and 1.0 are contributions from the polyhedra associated with chain ends. With the increase in temperature the peak in the distribution shifts to a larger value as expected from the increase in the system volume, but at the same time the distribution becomes considerably broader. At low temperature the contributions from chain end polyhedra, some 60–65% larger, are well separated from those associated with internal segments. As the distribution broadens at higher temperature, the subsidiary maximum due to chain end polyhedra becomes obscure, while the volume fraction of the system occupied by the chain end polyhedra increases. As is illustrated in Figure 2, a fairly sharp increase in the chain end polyhedra volume fraction occurs between $T = 2.0$ and 3.0, somewhat above the T_g ($T = 1.96$). A similar increase in the width of the part of the distribution associated with internal segments is also found above $T = 3.0$. These observations suggest that the broadening of the distributions may be associated not with the expansion of the system volume as a whole, which starts at the T_g, but rather with the availability of significant numbers of conformational transitions, which was found[15] to begin to occur, on the time scale of the simulations, only above $T = 2.6$. The observed larger polyhedron volumes associated with chain ends may not be construed as necessarily implying a larger free volume associated with chain ends, as is often assumed to explain, for example, the chain-length dependence of the glass transition temperature. Two neighbors of an internal segment are bound at a distance of C–C bonds, whereas only one neighbor of a chain end segment is so bound, all the others being held at a much larger distance of nonbonded interactions. This obviously necessitates a larger polyhedron associated with a chain end segment. The average nonbonded neighbor distance, moreover, increases with increasing temperature, thus also accounting for the

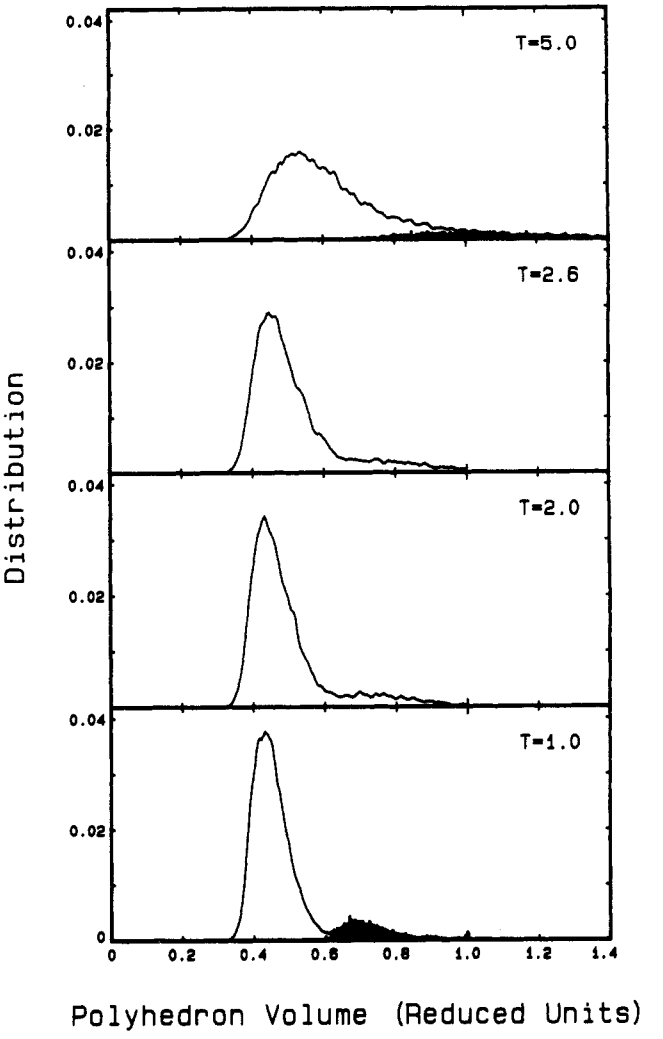

Figure 1. Distributions of volumes of Voronoi polyhedra at the indicated temperatures, which lie above and below the T_g (=1.96). The bar graphs indicate the contribution by Voronoi polyhedra belonging to chain ends.

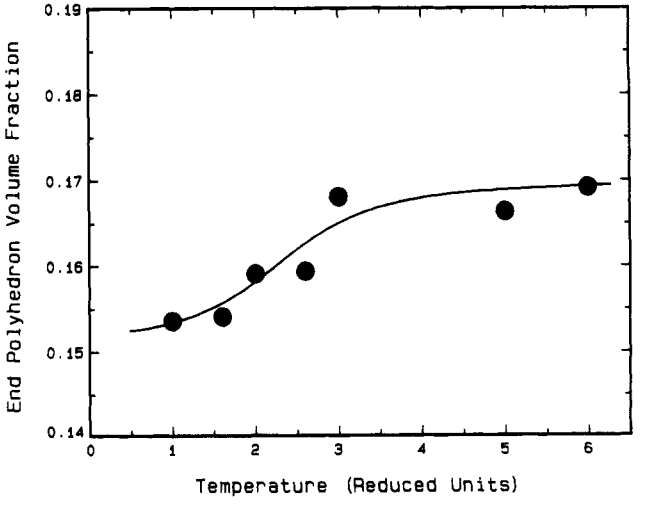

Figure 2. Temperature dependence of the volume fraction of Voronoi polyhedra belonging to chain ends.

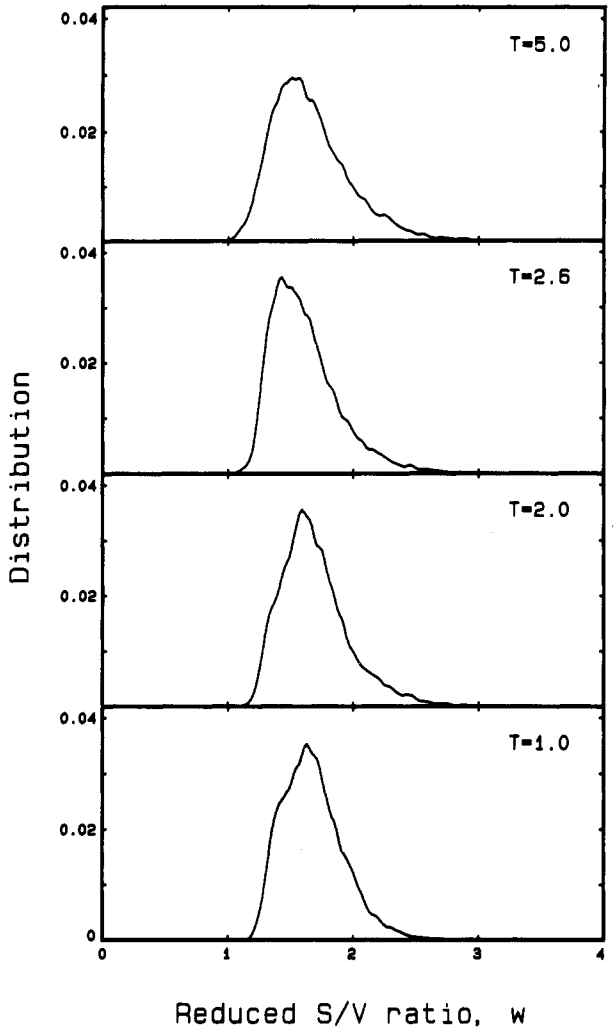

Figure 3. Distributions of the shape factor, w, of the Voronoi polyhedra at the temperatures indicated.

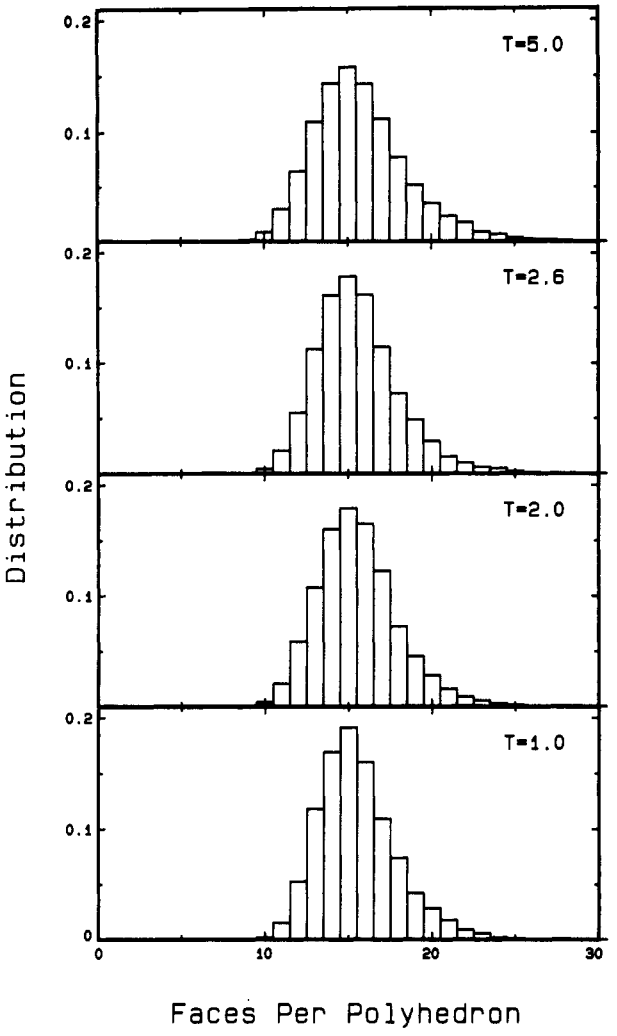

Figure 4. Distributions of the average numbers of faces per polyhedron for the four temperatures as in Figure 3.

observed increase in the volume fraction of chain end polyhedra.

Distributions of the shape factor w (surface to volume ratio) of the Voronoi polyhedra are illustrated in Figure 3 for the same temperatures as shown in Figure 1. The main peak located at around $w = 1.58$ at $T = 1.0$ and 2.0 shifts to lower values 1.45–1.50 at temperatures $T = 2.6$ and above, indicating that the polyhedra become slightly more symmetrical (more compact) at temperatures much above the T_g. The result at $T = 1.0$ suggests a bimodal distribution of polyhedra, the shoulder in the distribution occurring at about $w = 1.45$. It is tempting to speculate that this might suggest the presence of the higher temperature liquid structure embedded among the frozen low-temperature structure.

The average number of faces per polyhedron associated with an internal segment remains in the range 15.08–15.12 at all temperatures up to $T = 3.0$ and then rises only slightly to 15.30 at $T = 6.0$. The number of faces per end polyhedron rises slightly from 19.31 at $T = 1.0$ to 19.37 at $T = 2.0$ and to 20.31 at $T = 6.0$. Actual distributions of the number of faces per polyhedron are illustrated in Figure 4. The shape of the distribution remains unchanged through the temperature, except that the distribution becomes somewhat broader at higher temperatures. The number of edges per face shows even less sensitivity to temperature. The distribution can be described by saying that at all temperatures about 25% of face have 5 edges, and 4- and 6-edged faces contribute 21% each. In contrast to our results, the most abundant are 12-faced polyhedra and 4-edged faces in the Lennard-Jones monatomic liquid modeled by a molecular dynamics simulation.[21] This difference, indicating a larger number of neighbors to a polymer segment than to an atom in a monatomic liquid, finds a parallel in our earlier evaluation[13] of the radial distribution function. We found there that the number of neighbor segments in the "first coordinate shell" in our system was as many as 45–47, in contrast to the values 10–12 normally found in a monatomic system. The larger number of neighbors arises because in a chain molecule system two neighbors bound by covalent bonds are forced to remain around each segment at distances much closer than nonbonded interatomic distances.

(b) Cavity Volume and Its Distribution. The cavity-volume analysis is performed, as stated in Method, by prescribing a sphere of diameter D on every segment center and then evaluating the space not occupied by any of these spheres. A cavity is a contiguous region (a "pocket") of such unoccupied space. If the van der Waals diameter of a CH_2 unit is D_{vdW} and a small probe molecule of diameter D_p is imagined inserted into the system, then $D = D_p + D_{vdW}$ represents the diameter of the volume around each segment that is excluded to the probe molecule center. The results of cavity-volume analysis are presented below as a function of the "exclusion diameter" D varying from 1.0 to 2.0. When diffusion of small gas molecules through the polymer is of interest, they may readily be reinterpreted in terms of the probe molecule size $D_p = D - D_{vdW}$, where

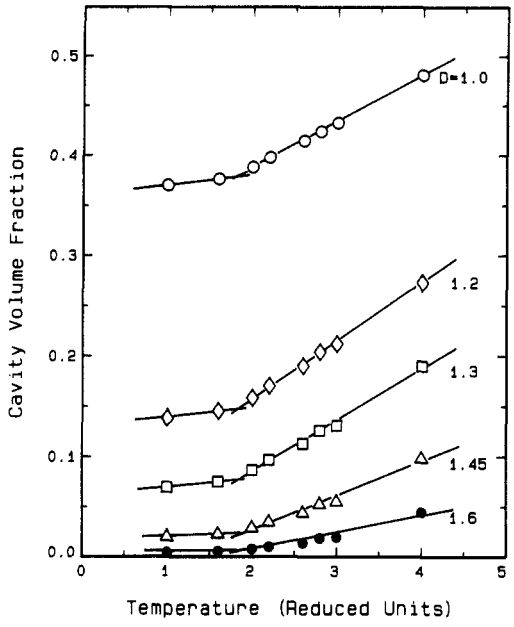

Figure 5. Variation with temperature of the volume fraction of cavities within the simulated bulk *n*-alkane systems as obtained when the exclusion diameter D is assigned the value indicated.

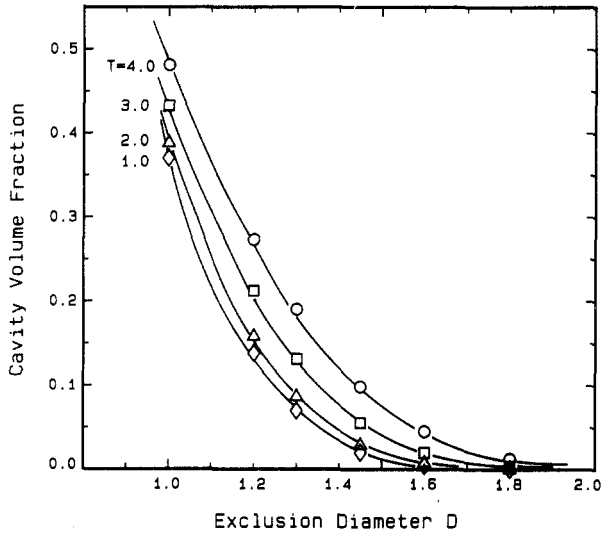

Figure 6. Cavity-volume fraction shown in Figure 5 replotted to show its dependence on the exclusion diameter D at the four temperatures indicated.

D_{vdW} is approximately equal to 1.0. The free volume itself can then be regarded as the unoccupied space accessible to molecules of D_p equal to zero.

Figure 5 illustrates the variation with temperature of the cavity volume, expressed as a fraction of the total system volume for D equal to 1.0, 1.2, 1.3, 1.45, and 1.6. Here, the behavior essentially parallels that of the total system volume, with a characteristic change in slope occurring at around the glass transition temperature (T = 1.96). In Figure 6, the data in Figure 5 are cross-plotted against D for the four temperatures T = 1.0, 2.0, 3.0, and 4.0. It shows that a probe molecule of D_p = 0.8 can only barely be accommodated even at temperature as high as T = 4.0, and no room is available for a probe molecule of D_p = 0.6 or larger at temperatures below the T_g. Plots similar to Figure 6 were presented in a recent work[22] analyzing the molecular models of polypropylene and poly(vinyl chloride) obtained by a molecular mechanics (energy minimization) technique. The cavity volume fraction at the T_g for D = 1.0 is equal to 0.388 in this work, while the free-volume fractions reported for the model of

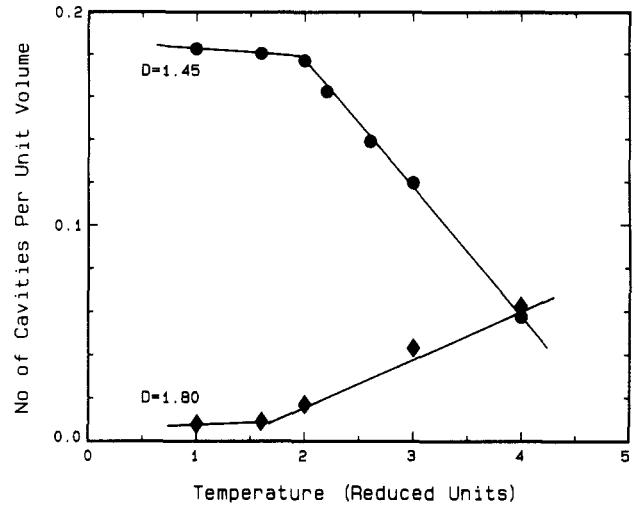

Figure 7. Variation with temperature of the number of cavities per unit volume for the two different values of the exclusion diameter D indicated.

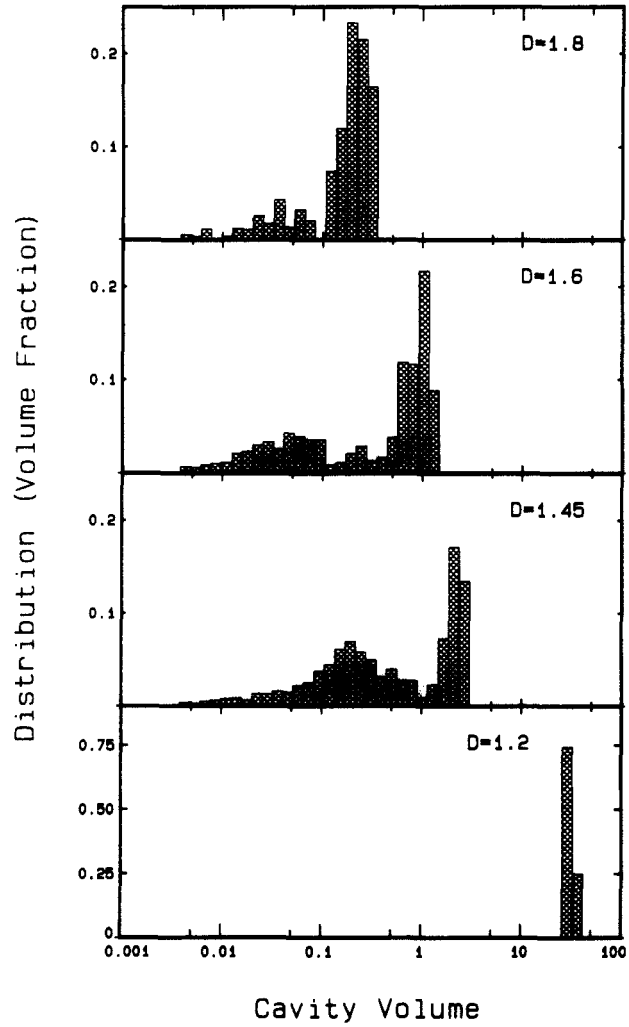

Figure 8. Volume fraction distributions of cavity sizes at T = 1.0 for the values of the exclusion diameter D indicated.

polypropylene at −40 °C and for the model of poly(vinyl chloride) at 70 °C (both below their respective T_g's) are 0.31 and 0.32, respectively.

The number of cavities per unit volume of the system shows interesting changes as the temperature is varied through the T_g, as shown in Figure 7 for D equal to 1.45 and 1.80. The number density of cavities remains fairly constant below the T_g, a consequence of the essentially

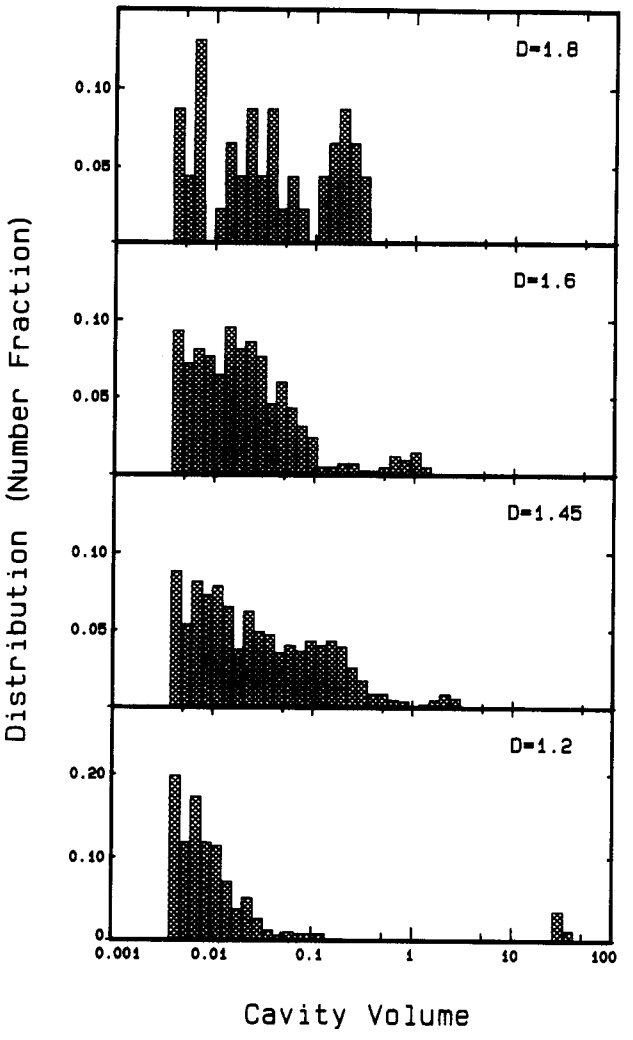

Figure 9. Data shown in Figure 8 now presented in terms of number fraction distribution.

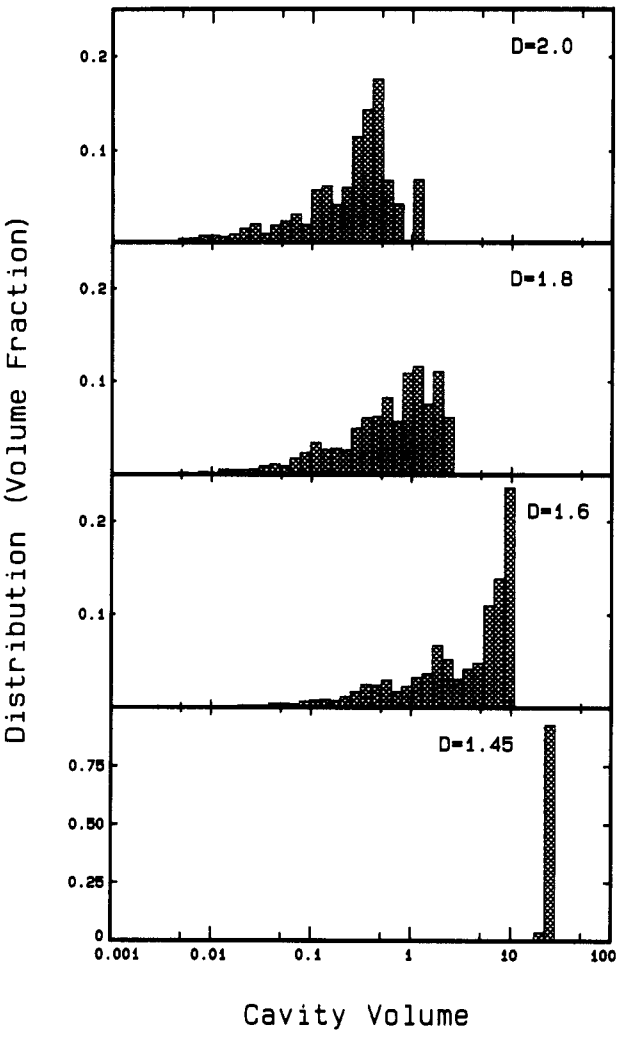

Figure 10. Volume fraction distributions of cavity sizes at $T = 4.0$.

frozen nature of the system. On the other hand, above the T_g, the number of cavities decreases with increasing temperature when the exclusion diameter D is small, while it increases with increasing temperature for a larger D. For the smaller D, the behavior arises due to coalescence of cavities as the overall volume expands with increasing temperature, while for the larger D, the cavities existing at low temperature are small and far from each other, and increasing the total system volume simply serves to create a number of additional small, isolated cavities. In principle, further increase in the system volume at higher temperatures than studied should cause the number of cavities for the larger D to decrease as these again coalesce to form larger cavities.

The cavities themselves exhibit broad size distributions, which have a bimodal or occasionally a trimodal character. This is illustrated in Figure 8, which shows the volume fraction distributions of cavities of various sizes for the system at $T = 1.0$. When the value assigned to D is reduced from 1.8 successively to 1.6, 1.45, and 1.2, the average size of the cavities increases but the essentially bimodal character of the distribution remains. For $D = 1.2$ the volume fraction distribution is overwhelmed by cavities of extremely large sizes, but the number fraction distribution, illustrated in Figure 9, shows the presence of small ones as well. Figure 10 gives the volume fraction distributions above the T_g at $T = 4.0$. With the increased overall cavity volume available at the higher temperature, the average cavity size is now considerably larger for a given D value, but the distributions remain very broad, although the clustering of the distribution into two or three distinct size classes is now less obvious.

Some idea of the shape of these cavities can be obtained by plotting the distribution of the reduced S/V ratio, w, as is illustrated in Figure 11. The distribution is evidently very broad, covering the whole range from the very compact and rounded ones ($w = 1$) to very elongated or irregular ones ($w > 4$). If we weigh the distributions given in Figure 11 according to the volume of the cavity, thus producing volume fraction distributions, the result shown in Figure 12 is in general shifted to much smaller w values, and this indicates that it is the larger cavities that are more rounded and compact in shape.

(c) Cavity-Volume Fluctuation Dynamics. These cavities are obviously not static, and they constantly change their shape and size and break up and merge together, as the molecules themselves change shape and move around. To analyze such dynamics properly, one needs to perform visual observation of the motions by graphic techniques as well as evaluation of statistical averages such as time-correlation functions. We have performed only a very limited visualization study in this work, but the little preliminary result obtained is already very illuminating and is reported here.

Even at a temperature as low as $T = 1.0$, which is much below the T_g, a considerable degree of motion is observable with the cavities. Figure 13 gives the projection of the cavities on $X-Y$ plane at intervals of 5 ps (2.5 reduced units), obtained at $T = 1.0$ and for $D = 1.8$. Three different

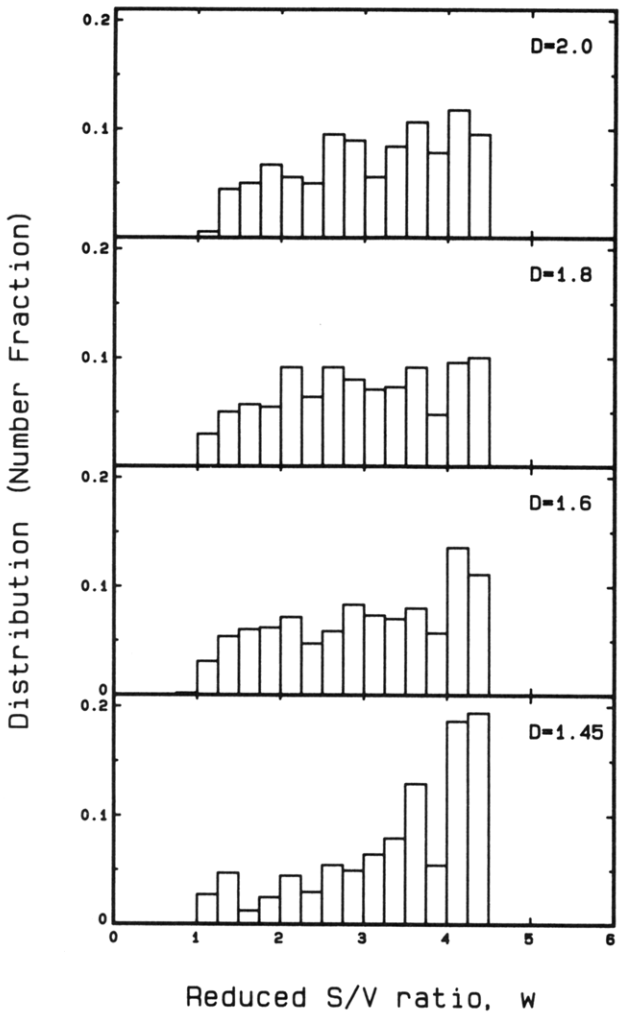

Figure 11. Distributions (number fractions) of the shape parameter w of cavities obtained under the same conditions as in Figure 10.

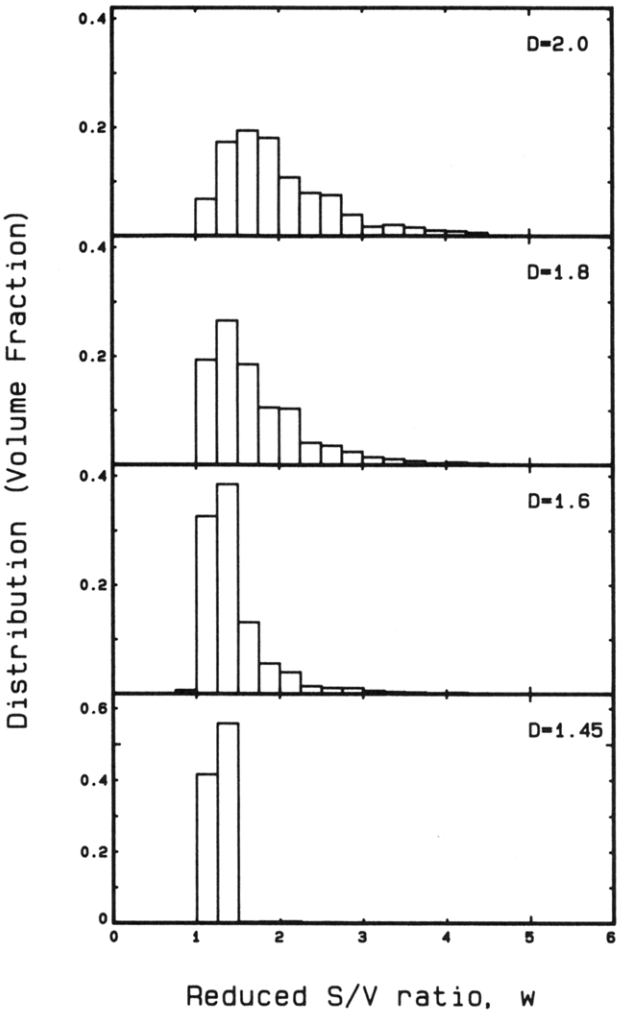

Figure 12. Distributions of the shape parameters w, which have been weighted according to the cavity volume, for the same conditions as in Figure 11. The average values of w are now greatly reduced, indicating that the larger cavities, on the average, possess smaller values of w.

cavities are identified and are distinguished by different shadings. The time-lapse projections show that at T = 1.0 there still persists a large amplitude, low-frequency motion of molecules, which gives rise to the waxing and waning of the cavities. Despite the changes in the shape and size with time, they are not diffusing away, and in fact after having disappeared altogether in the 25 ps frame, they reappear later at about the same place as they were before and remain there until the end of the run lasting 120 ps. This suggests that there is a spatial inhomogeneity in density, which does not decay, on the time scale of our simulation, even in the glassy state.

The result illustrates that a glass is far from being a frozen, immobile structure but rather retains a considerable degree of molecular motions, which have to be taken into consideration in understanding its properties. Previously, our small-angle X-ray scattering study of glassy polymers led us to conclude[26,27] that the density inhomogeneities present in glass consist of two components, the dynamic one due to residual molecular motions and the quasi-static one, which was frozen in at the time of glass formation at the T_g. The present result lends support to such a conclusion.

Concluding Remarks

In the present work, we have studied the distribution of occupied and unoccupied volumes within n-alkane systems as they are quenched from the supercooled liquid

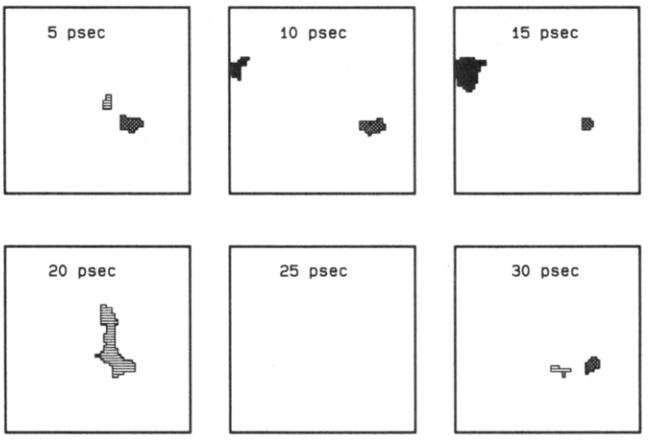

Figure 13. Projections on the X–Y plane of cavities obtained at T = 1.0 and D = 1.8 at successive time frames separated by 5 ps.

to the glassy state. The Voronoi tessellation analysis shows that the distribution of polyhedra volumes is broad at high temperature but becomes narrower as the temperature is lowered through the T_g. The distribution of volumes of cavities, formed when the alkane segments are replaced by hard spheres of diameter D, is extremely broad and often exhibits a bimodal or trimodal character. These cavities change shape and size with time; even at tem-

peratures much below the T_g, persistent low-frequency molecular motions produce waxing and waning of the cavities. When a cavity disappears, it later reappears at about the same position, reflecting a globally frozen nature of the material.

Examination of the various features presented in Figures 1–13, however, does not reveal any obvious characteristics that can be pointed out as clearly distinguishing the glassy state from the liquid state. In the study of monatomic or small-molecule liquids and glasses experimentally or by computer simulation, it has commonly been observed[23] that the second peak of the radial distribution function splits into two subpeaks at low temperatures, and this split second peak is often regarded as a signature of the glassy state. In their study of the Lennard-Jones liquid, Jonsson and Andersen[24] report that on cooling through the T_g the structure changes slightly above the T_g and local 5-fold symmetry becomes more prominent. If one were to interpret the glassy transition as marking the percolation threshold of either free-volume cavities or clusters of liquidlike (as against solidlike) cells in the liquid, as the theory by Cohen and Grest[25] implies, then one ought probably look for some structural features that change at the T_g and thus distinguish glass from liquid. We have not, however, succeeded in finding any characteristic features of this sort in this work. In our earlier publication[13] we noted the splitting of the second peak of RDF occurring in our alkane systems only at temperatures much below the T_g, leading us to conclude that the splitting is associated with a low-temperature structure and not necessarily with a glass structure. The failure to find structural characteristics distinguishing glass and liquid is not really surprising when it is considered that the discontinuity at the glass transition temperature is not in the first-order quantities such as density and entropy but only in the temperature coefficients of such quantities. Accordingly, in the present study, only the temperature coefficients of the cavity volume or the number density of cavities (illustrated in Figures 5 and 7) are found to undergo discontinuous change at the T_g.

Diffusion coefficients of small gas molecules, rate of positron annihilation, and kinetics of isomerization of probe molecules are all quantities that undoubtedly are closely related to the free-volume content of the material. The latter two are in fact utilized as a means of determining the free-volume distribution in polymers, but analysis of the experimental results to yield quantitative evaluation of free volume may require a better "calibration" of the techniques against the free volumes obtained by means of simulations such as ours. Such a comparison is also likely to tell us the importance of dynamics as well as statics of free volume and its distribution in governing these experimentally observable quantities.

Acknowledgment. This work was supported in part by NSF Grants DMR8520921 and DMR8909232. The computation reported in this work was performed on a CRAY Y-MP at the Pittsburgh Supercomputer Center and Ohio Supercomputer Center.

References and Notes

(1) Dootillte, A. K. *J. Appl. Phys.* **1951**, *22*, 1471.
(2) Fox, T. G.; Flory, P. J. *J. Appl. Phys.* **1950**, *21*, 581; *J. Polym. Sci.* **1954**, *14*, 315.
(3) Simha, R.; Boyer, R. F. *J. Chem. Phys.* **1962**, *37*, 1003.
(4) Struik, L. C. E. *Physical Aging in Amorphous Polymers and Other Materials*; Elsevier: New York, 1978.
(5) Kovacs, A. J. *Fortschr. Hochpolym.-Forsch.* **1964**, *3*, 394.
(6) Kobayashi, Y.; Zheng, W.; Meyer, E. F.; McGervey, J. D.; Jamieson, A. M.; Simha, R. *Macromolecules* **1989**, *22*, 2302.
(7) Yu, W. C.; Sung, C. S. P.; Robertson, R. E. *Macromolecules* **1988**, *21*, 355; **1988**, *21*, 365.
(8) Victor, J. G.; Torkelson, J. M. *Macromolecules* **1987**, *20*, 2241; **1987**, *20*, 2951; **1988**, *21*, 3490.
(9) Voronoi, G. F. Z. *Reine Angew. Math.* **1908**, *134*, 198.
(10) Ichimura, I.; Ogita, N.; Ueda, A. *Jpn. J. Phys. Soc.* **1978**, *45*, 252.
(11) Hiwatari, Y. *J. Chem. Phys.* **1982**, *76*, 5502.
(12) Rigby, D.; Roe, R. J. *J. Chem. Phys.* **1987**, *87*, 7285.
(13) Rigby, D.; Roe, R. J. *J. Chem. Phys.* **1988**, *89*, 5280.
(14) Rigby, D.; Roe, R. J. *Macromolecules* **1989**, *22*, 2259.
(15) Rigby, D.; Roe, R. J. In *Computer Simulation of Polymers*; Roe, R. J., Ed.; Prentice Hall: New York, in press.
(16) Allen, M. P.; Tildesley, D. J. *Computer Simulation of Liquids*; Oxford University Press: New York, 1987.
(17) Finney, J. L. *Proc. R. Soc. London* **1970**, *A319*, 459, 479.
(18) Brostow, B.; Dussalt, J. P.; Fox, B. L. *J. Comput. Phys.* **1978**, *29*, 81.
(19) Tanemura, M.; Ogawa, T.; Ogita, N. *J. Comput. Phys.* **1983**, *51*, 191.
(20) Medvedev, N. N. *J. Comput. Phys.* **1986**, *67*, 223.
(21) Hsu, C. S.; Rahman, A. *J. Chem. Phys.* **1979**, *71*, 4974.
(22) Shah, V. M.; Stern, S. A.; Ludovice, P. J. *Macromolecules* **1989**, *22*, 4660.
(23) Waseda, Y. *The Structure of Non-Crystalline Materials, Liquids and Amorphous Solids*; McGraw-Hill: New York, 1980.
(24) Jonsson, H.; Andersen, H. C. *Phys. Rev. Lett.* **1988**, *22*, 2295.
(25) Cohen, M. H.; Grest, G. S. *Phys. Rev.* **1979**, *B20*, 1077.
(26) Roe, R. J.; Curro, J. J. *Macromolecules* **1983**, *16*, 428.
(27) Roe, R. J. *J. Chem. Phys.* **1983**, *79*, 936.